Experimental Investigation of Flow Control Using Blade End Slots in a Highly Loaded Compressor Cascade

Yumeng Tang[1],Yangwei Liu[1,2]*, Lipeng Lu[1,2], Huawei Lu[3], Ming Wang[4]

ISROMAC 2017

International Symposium on Transport Phenomena and Dynamics of Rotating Machinery

Hawaii, Maui

December 16-21 2017

Abstract

A detailed experimental investigation is conducted to suppress three-dimensional (3D) corner separation by a proposed passive control method using blade end slots in a highly loaded high-speed compressor cascade. Experiments are carried out under a wide range of incidence angles at Ma=0.59 using blades with and without blade end slots, respectively. Based on the experimental results, extensive comparisons show that the proposed method using blade end slots can efficiently suppress the 3D corner separation and broaden the effective operating range in the highly loaded high-speed compressor cascade. The total pressure loss is significantly reduced under most conditions. The reduction of total pressure loss in the measurement plane is as high as 18.4%, 20.6%, 24.3% and 39.4% at the incidence angle of -1.69˚, 0˚, 2˚ and 4˚, respectively. Furthermore, spanwise distributions of the pitch-averaged total pressure loss and deviation angle as well as the 3D flow field structures are analyzed to reveal the flow control mechanisms using blade end slots. The blade end slots can generate self-adaptive high momentum jet flow through the pressure difference from blade pressure and suction surface. These jet flows from the blade end slots effect downstream along the blade suction surface and significantly increase the flow momentum in the corner region. The main secondary vortex structures are suppressed by the high momentum jet flow; the 3D corner separation is reduced, and the two-dimesionality in the mid-span region is enhanced.

Keywords

Compressor Cascade — Corner Separation — Flow Control — Blade End Slot

[1]*National Key Laboratory of Science and Technology on Aero-Engine Aero-Thermodynamics, School of Energy and Power Engineering, Beihang University, Beijing 100191, China*

[2]*Collaborative Innovation Center of Advanced Aero-Engine, Beihang University, Beijing 100191, China*

[3]*Marine Engineering College, Dalian Maritime University, Dalian 116024, China*

[4]*Shenyang Engine Design and Research Institute, Aviation Industry Corporation of China, Shenyang 110015, China*

***Corresponding author**: liuyangwei@126.com

INTRODUCTION

Three-dimensional (3D) corner separation is identified as an inherent flow feature in the blade suction surface and endwall conjunction of the axial compressors [1]. As Denton established, the secondary flows in the blade-endwall junction causes about one-third of losses in axial compressor [2]. The pressure gradient transverse to the flow direction affects both separation and loss in the compressor flow [3]. As the development of modern jet engines, the application of highly loaded blade is desired for the purpose of reducing weight as well as lowering manufacturing and maintenance costs. However, increasing blade loading inherently aggravates the corner separation and induces higher losses. Thus, various control methods [4-16] have been proposed to suppress corner separation in axial compressors, especially the highly loaded ones.

Previous studies demonstrate that the 3D corner separation in a highly loaded compressor could be suppressed through active or passive flow control methods. Some active flow control methods, such as boundary layer aspiration [4, 5], plasma [6, 7] or fluidic actuators [8], synthetic and continuous jets [9], vortex generator jets [10], can reduce corner separation loss and improve compressor performance; however, these methods require additional devices. Compared to active flow control methods, passive flow control approach earns for its simplicity and cost effectiveness. Some passive flow control methods, such as blade center slots [11] or whole span slot [12], sidewall grooves [13], and vortex generator [14] have been used and also shown some benefits. Tangential blowing over the profile suction surface is supplied by blade center slots to increase boundary layer momentum and therefore delaying or preventing separation, while the two-dimensional separation at the mid-span region is enlarged, resulting in the massive deflection at mid-span [11]. The vortex generator devices produce strong vortices that enhance the mixing between the main flow and the decelerated boundary layer, reducing the corner separation and total pressure loss therefore [14]. Generally speaking, current passive flow control methods have some limitations, especially do not universally suitable for all the operating conditions.

Nerger et al experimentally studied an active flow control method and concluded that steady tangential blowing over the profile suction surface can increase boundary layer momentum and therefore delaying or preventing 3D corner separation [15], while extra blowing jet is demanded and the decrease of the total pressure loss is possible for a few operating points only. Accounting for the shortage of active flow control blowing and to utmost its advantage, Liu et al. recently proposed an adaptive passive flow control method through slot established at the end of the blade [16].

Numerical investigations of the blade end slots on a low-speed prescribed velocity distribution (PVD) cascade reveals a progressive perspective in improving compressor performance.

The present paper experimentally investigates the effects of blade end slots on the 3D corner separation in a highly loaded high-speed compressor cascade under a wide range of incidence angles at Ma=0.59. Based on the experimental results, extensive comparisons are conducted to assess the effectiveness. The spanwise distributions of pitch-averaged total pressure loss and deviation angle as well as the 3D flow field structures are then analyzed to reveal the flow control mechanisms using blade end slots.

1. CONFIGURATIONS

The target blade investigated is a state-of-art highly loaded high turning one, which is designed for a typical subsonic Mach number that encountered in modern multi-stage axial compressor. Pre numerical investigations indicate that the datum blade tends to fail as a consequence of 3D corner stall on the section side under high positive incidence angles, accompanied with significant increase of under-turning. While the proper designed end slotted blade provides a more uniformed outflow with less deviation angle due to the suppression of 3D corner separation, and the loss is also reduced. The high adverse pressure gradient in the cascade passage as well as the interaction between the thick boundary layer from the endwall and blade surface are the main causes for the corner separation. The geometry of the end slots section is optimized numerically before experiments under inconsistent incoming conditions. As Ashley et al. established, the endwall boundary layer state has a significant influence on the 3D corner separation [17], though differences on the endwall boundary layer thickness makes the designed end slots geometry is not the optimist one under the current experimental conditions, massive benefits in performance still reward at last.

1.1 Datum Blade Geometry

The datum configuration is a highly loaded high-turning compressor cascade, whose profile is cut off at the middle span of a modern compressor stator. Table 1 presents the general geometry parameters of the datum blade together with its aerodynamic design conditions.

Table 1. Geometry Parameters of the Datum Blade

Compressor Cascade	Values	Units
Chord length c	55	[mm]
Solidity c/t	1.52	[-]
Aspect ratio h/c	1.82	[-]
Inlet mental angle	41.91	[°]
Stagger angle	21.7	[°]
Camber angle	52.94	[°]
Outlet mental angle	94.85	[°]
Design *Ma* number	0.59	[-]

The experimental blade has an aspect ratio of 1.82 due to the height of the tunnel cross section. The turning-angle of the blade is as large as to approximately 53 degree with the D-factor approaching 0.55. The designed Mach number is equal to 0.59, which represents a typical subsonic Mach number encountered in modern multi-stage axial compressor, so the transferability to the real turbomachines is possible.

1.2 End-Slot Blade Configurations

The end slotted blade shares the same general geometry parameters with the datum one and the experimental conditions also remains.

The 3D model of the end slotted blade is exhibited in Figure 1. In correlation to which, Figure 2 demonstrates the cut-off geometry of the datum section (in black) and the end slot section (in red).

Figure 1. 3D Model of the End slotted blade

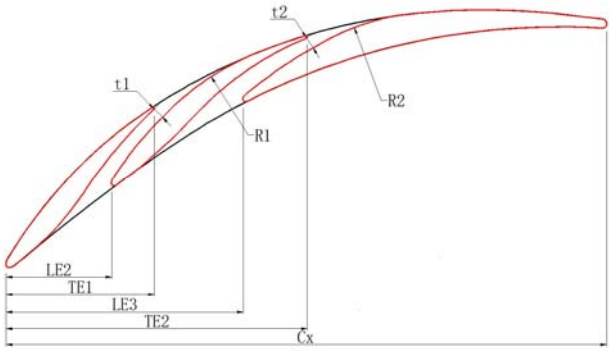

Figure 2. Cross Section Configurations of the Datum and End Slotted Blade Geometry

The profile of the end slots is successively derived from the datum configuration, both of them can connect seamless. Considering that the Coanda effect occurs when a free stream flow above a curved surface is entrained by a parallel high momentum wall jet tangential along the curved surface, a Coanda radius corresponding to slot throat width is integrated tangentially with the downstream profile of the suction surface. As it proved previously that the Coanda jet remains attached to the curved surface as the result of the balance between the centrifugal force around the curved surface and the sub-

ambient pressure in the jet sheet [18]. The momentum of the jet out of the blade end slots energizes the downstream suction surface boundary layer and gains its ability to resist separation caused by the adverse pressure gradient along the curved surface. Goodhand et al. emphasized the sensitivity of geometry deviation on the loss production [19]. So all the curves are smoothly blending and the leading-edge (LE) is well-treated. The total chord length in the end slotted section remains the same with the datum one to minimize the variation in geometry. Each trailing-edge (TE) radius per slot-including section is limited to 0.1 mm to restrain aggressive wake mixing losses. Both end slots originate from the endwall and occupy 20% of the whole span height, effecting the blade-endwall conjunction only.

The end slots section is coupled with the middle datum one and is divided into three individual elements by two curve shaped slots. Those three elements are named sec1, sec2, sec3 respectively from LE to TE. The main geometric designing parameters of the end slots section are summarized in Table 2.

Table 2. Geometry Parameters of the End-Slots Section

Section	Feature	Relative Position/ Values []
sec1	LE1	0%Cx
	TE1	25%Cx
slot1	AO1	7.4%Cx
	t1	1 [mm]
	t1/R1	0.043
	h1	20%H
sec2	LE2	17.6%Cx
	TE2	50%Cx
slot2	AO2	10%Cx
	t2	1 [mm]
	t2/R2	0.05
	h2	20%H
sec3	LE3	40%Cx
	TE3	100%Cx

The LE and TE positions are necessary parameters to depict slot, and the slot shapes are characterized by the axial overlap (AO) together with the throat width (t). The LE of section 1 (sec1) is contacted with the LE of the datum blade, and the TE of it is located in 25%Cx (Cx stands for axial chord length, the position is related to datum LE). The LE and TE for sec2 is seated 17.6%Cx and 50%Cx respectively, and the LE for sec3 lies in 40%Cx position. The TE of sec3 is coupled with the datum blade. AO is the axial distance between the rear airfoil LE and the indicated TE. The throat width t in the slot outlet and the slot height h are vital to the determination of adaptive mass flow rate. Small ratios of the slot throat width and radius t/R which promotes the Coanda effect is chosen to delay flow detachment and to increase total turning.

The effective entrainment effect is highly depended on the slot out position, alternatively, determined by the local pressure of the slot out on the suction side of the blade. The integral total pressure in the slot inlet region can be approximated by the incoming flow total pressure integrated from the identical height of the slot mostly, if non local separation occurs. The throat velocity in the slot outlet would be estimated through local pressure in a certain slot geometry. Defining the slot inlet total pressure as P_{t1} and the pressure neighboring the slot throat as P_2, the local tangential out flow velocity V_t can be estimated as

$$V_t = \sqrt{C_a R T^* \left[1 - \left(\frac{P_2}{\sigma P_{t1}} \right)^{C_b} \right]} \tag{1}$$

where T^* is the total temperature, R is the ideal gas constant, C_a and C_b are constant that assigns 7 and 2/7 respectively. σ is the empirical determined total pressure recovery coefficient of the slot, assuming 0.98 if no separation occurs internal the slot. The mass flow rate of the slot jet could be preliminary evaluated as

$$\dot{m}_{slot} = K \frac{\sigma P_{t1}}{\sqrt{T^*}} t \cdot h C_d \lambda_2 \left(1 - C_f \lambda_2\right)^{c_g} \tag{2}$$

$$\lambda_2 = \frac{V_t}{\sqrt{C_a C_f R T^*}} \tag{3}$$

where $K = 0.0404\ \mathrm{K}^{\frac{1}{2}}\mathrm{sm}^{-1}$, C_d, C_f, C_g are constant assigned with 1.58, 1/6, 2.5. t and h stands for the width and height of the slot throat respectively.

The jet flow velocity and the mass flow rate of the blade end slots are adaptively based on the local flow parameters, since the flow field is determinate.

2. EXPERIMENTAL SETUP

The main phenomenon this study concerned is the 3D corner separation influenced by blade end slots under different incoming flow incidence conditions.

2.1 Experimental Facility

All the experiments are carried out in a high-speed linear compressor cascade tunnel. Consecutive air is supplied to the test section after cooling, which is driven by a high-pressure radial compressor. The supplied incoming flow goes through several inflowing values, a silencer, a diffusor, a settling chamber and a nozzle by step. Mach number of approximately 0.59 and Reynolds number of up to 0.72×10^6 could be obtained.

The test section has a cross section of 100mm in height and an adjustable range more than 260mm in width. Eight arraying blades are adopted to guarantee periodic conditions in the pitchwise, and the fifth blade from the top was chosen as the testing one. The arrangement of the test rig is shown in Figure 3. The blade carriers are mounted on a ratable disk, which enables a continuous change of the incoming angle. Depending on the incoming flow angle, the vertical height of the test section would be adjusted by moving the inlet floor top and bottom. A three-hole probe with a diameter of 1.5mm is emplaced upstream to monitor the incoming flow Mach

number and the real flow angle. Variation in the incidence is adjusted according to the monitoring value of the three-hole probe to guarantee the incoming flow angle actual. Adjustment for the incoming flow Mach number is achievable by the valve opening accommodations. Non aspiration devices is equipped in the test rig that the developed incoming flow boundary layer migrates directly to the blade passage along the side wall.

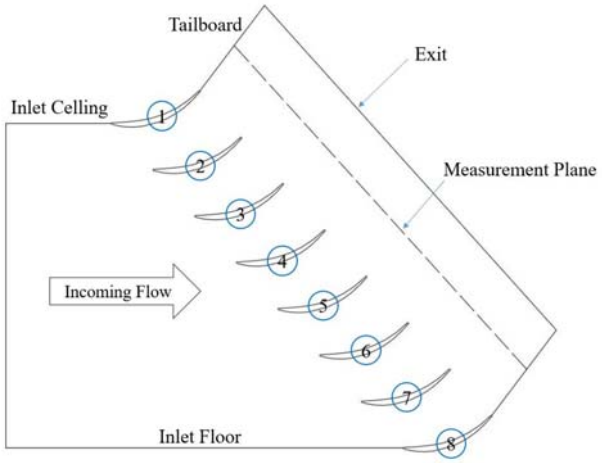

Figure 3. Sketch of the Test Section

The experimental blades are fixed to the endwall without gap and airproofed by melt adhesive outside the endwall. The test rig of the end slotted blade is arranged the same. The end slots is symmetric on both sides of the blade with corresponded endwall filled up. Only half of the passage in spanwise was covered in the measurements due to the completely symmetric flow conditions.

2.2 Experimental Measurement

Measurements are made by a calibrated five-hole probe in the plane 60% chord length behind of the TE under different incoming flow incidence angles. An extensive meshy measurements are made through the transverse of the probe along pitchwise and spanwise. More than one blade passage range, 110% pitch length, is covered. Meticulous measurement is conducted in the wake and separation regions to better capture the loss. The diameter of the probe is 2mm, occupying the proportion less than 0.05% of the full outflow area.

In the measurements, the detected five-hole probe is fixed to the movement driving by a stepping motor. A digital pressure-scanivalve system DSA3217 is adopted for pressure collection, and the detected pressure signal is automatically records by PC with special software and the probe movement is commanded by a given procedure through controlling the traverse mechanism. Those acquisitions are the valves against the atmospheric one, namely the gage pressure. For each collection, the corresponding atmosphere pressure and temperature is also recorded. The scan frequency of the scanivalve system is 5 frames per second, 20 frames sampled each point and the averaged values are outputted finally.

Test error comes from the probe calibration error, transducer error and the measurement error. The accuracy of the five-hole probe is within 0.1%, the pressure transducer error is about 0.05%, and the measurement error is regarded as 0.05%. Error under 0.2% exists when recovering the local total pressure and static pressure values through interpolating from the five-hole probe detected ones. Thus, the total error for the data acquisition is no more than 3% at last. The flow angle capture can be thought effective within the range of ±30 degrees.

To quantify losses, the total pressure loss coefficient is defined as

$$Yp(x,y)=\frac{\overline{p}_{t1}-p_t(x,y)}{\overline{p}_{t1}-\overline{p}_{s1}} \tag{4}$$

where $\overline{p}_{t1}$ stands for the incoming flow total pressure, $\overline{p}_1$ is the incoming flow static pressure. The total pressure of the measured point (x,y) is denoted as $p_t(x,y)$. The total pressure and the static pressure that detected by the three-hole probe one at chord length ahead of the LE are used to represent incoming flow features. The total pressure loss coefficient is calculated for every measurement. Besides, the distribution of velocity and flow angle is also obtained through the measurements of the five-hole probe.

Mass flow average is used when evaluating the whole losses or the pitchwise averaged losses. The density is solved under the assumption of constant total temperature. The averaged total pressure loss coefficient is obtained by

$$Yp(x,y)_{avg}=\frac{\int Yp(x,y)\rho(x,y)\left|\vec{v}(x,y)\cdot d\vec{A}\right|}{\int \rho(x,y)\left|\vec{v}(x,y)\cdot d\vec{A}\right|} \tag{5}$$

Only pressure and temperature are detected in the experiments. The uncertainty for the three-hole probe or the five-hole probe highly depends on the relative probe inflow angle. Considerable precision can be assured within the inflow angle divergence of 30 degrees, thus the uncertainty is negligible under smaller angles. Since the inflow angle divergence is almost within the range of 30 degrees, the orientation error is not considered.

3. RESULTS AND DISCUSSION

It is already described former that the end slotted blade is utilized to suppress the extent of 3D corner separation, so comparisons are made for both datum and end slotted blade under the corresponded varying incoming flow conditions. Comparisons of the typical experimental results are analyzed.

3.1 Performance over the Range of Operation

To evaluate the blade end slots effects over the operating range, performances in both design and off-design conditions are compared.

The mass-weighted averaged total pressure loss coefficient for both datum blade and the end slotted blade varying with the incoming flow angle are depicted in Figure 4.

Obvious loss reduction by the blade end slots can be seen in comparison with the datum one. The critical incidence where the loss steeply increased can be thought as the surge or choke margin of the blade, and the incidences within the

margin can be regarded as effective operating range. For the datum blade, the effective operating range is narrow, mainly occupies negative incidences from -8˚ to -4˚, under which incidences the aerodynamic performance is not superior. Deterioration in the loss appears above the incidence -1.69˚ or below -8˚. The total pressure loss grows slightly when the incidence varies from -1.69˚ to 2˚, inasmuch as the transformation of 3D corner separation to mid-span separation.

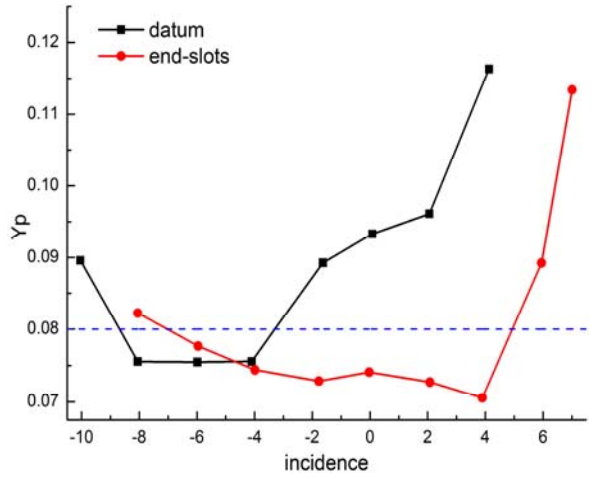

Figure 4. Total Pressure Loss over the Range of Operation

The employment of the end slotted blade shows prominent potential in extending the effective operating range positively forward. Considerable low total pressure loss could be achieved by end slotted blade under the incidence range of -4˚ to 4˚. Figure 5 displays the averaged relative loss coefficient, whose definition is

$$\Delta\overline{Yp} = \frac{\overline{Yp}_{datum} - \overline{Yp}_{slot}}{\overline{Yp}_{datum}} \quad (6)$$

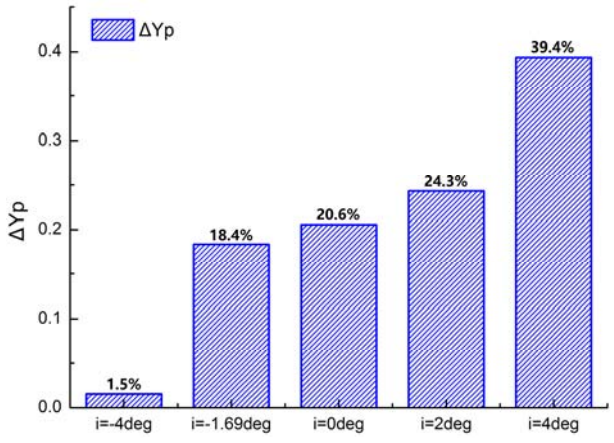

Figure 5. Relative Loss Coefficient over the Range of Operation

Relatively high benefit rewards under positive incidence conditions, where the corner stall dominates in the loss generation for the datum blade. Yielding a maximal total pressure loss of 39.4% related to the datum blade can be reduce by end slotted blade, due to the mitigation of 3D corner separation.

3.2 Spanwise Distribution of Pitch-Averaged Flow Parameters

To analyze quantitatively, comparisons are made through the spanwise distribution of pitchwise averaged total pressure loss coefficient and deviation angle.

3.2.1 Total Pressure Loss

The spanwise distribution of the total pressure loss coefficient for both datum blade and end slotted one are illustrated in Figure 6.

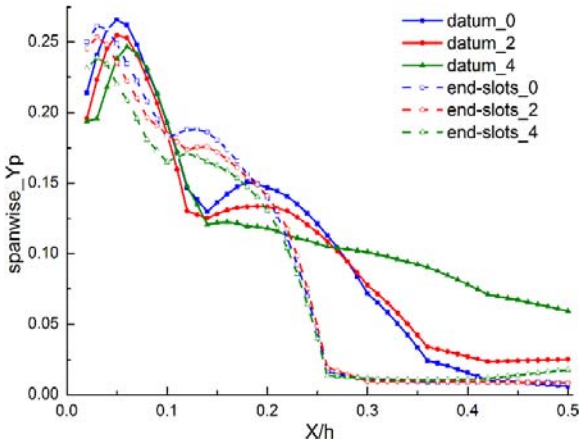

Figure 6. Spanwise Distribution of Pitch-Averaged Total Pressure Loss at the Measurement Plane

Peak values of the total pressure loss seat where the corner separation flow dominates. Two relatively large total pressure loss peaks are found for both datum blade and end slotted one in accordance to the distribution of low momentum fluid in the total pressure loss contours displayed farther. More than two thirds of the passage is blocked by the low momentum flow structures in the datum blade passage, with the high loss peaks situated approximating 8% and 20% span height, while the peak location reduced to about 4% and 15% span for the end slots blade together with the proportion of high loss region significantly reduced. Loss for the end slotted blade, interval the 10% to 25% span range, is high, due to the outflow slot height which occupied 20% of the blade span, proving that this slot design scheme is not the optimist under this experimental incoming boundary layer thickness.

Loss in the mid-span region reflects the wake mixing. Boundary layers from the blade suction surface and pressure surface gather in the TE and create the wake vortex structure together. The wake vortex moves downward and dissipates to internal energy through interactions under the viscosity effect. The total pressure and velocity that the wake owes is quite small, leading to a strong mixing in the wake main-flow conjunction, together with high dissipations.

It can be clearly seen from Figure 6 that the wake loss of the end slotted blade changes little with the incidence and keeps far less than that of the datum one. As mentioned in the

following chapter that the blade end slots enhances the two-dimensionality in the mid-span region of the blade.

3.2.2 Deviation Angle

The deviation angle distribution along the spanwise demonstrates the flow deflection influenced by the 3D corner separation. Figure 7 shows the comparison of pitchwise averaged deviation angle at the measurement plane along the blade height, both datum and end slotted results are presented. Mass weighted average in the pitchwise is used in the processes. The negative valve mirrors the over turning and the positive value corresponds under turning. As it described in the classical secondary flow theory that the over turning happens close to the endwall while the deficit in turning occurs away from the endwall due to the blockage caused by corner separation.

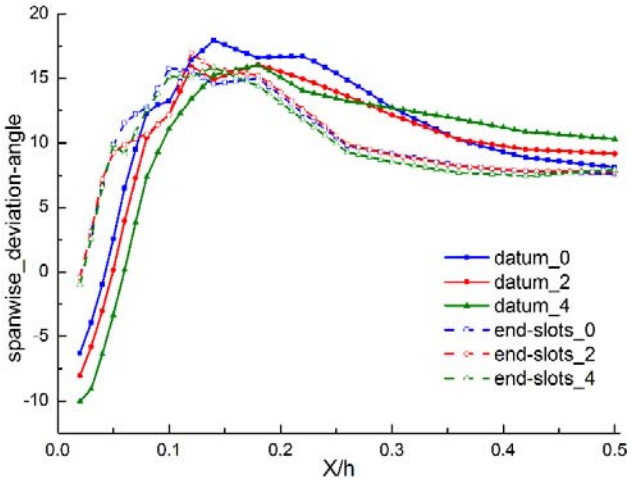

Figure 7. Spanwise Distribution of Pitch Averaged Deviation Angle at the Measurement Plane

Seen from Figure 7 that the deviation angle distribution is significantly reduced and uniformed by blade end slots above 10% span height. Though enlargement in the deviation angle exists near the endwall, resulting from the end slots jets, the increased degree is not obvious. As it mentioned previously that the designed jet flow from the slot outs has the Coanda effect that keeps attached on the blade suction surface. These distribution of the deviation angle near the endwall reveals that small separation is induced additionally by the end slot jet. The blockage caused by the low momentum fluid at the corner increases the flow turning ranging from 10% to 25% span height for the end slotted blade and 10% to 35% span for the datum blade. The adaptive jet flow from the blade end slots brings the blocked low momentum fluid downstream, restraining its migration along the spanwise, thus the flux of the mid-span region is substantially improved. Conclusions can be drawn from Figure 7 that the blockage is significantly mitigated by the blade end slots, as a consequence, the main flow region with better properties enlarges and the whole capacity is improved.

3.3 Total Pressure Loss Contours

Variation in the incoming flow angle changes the flow turning inside the blade passage, resulting in the altering in the distribution of pressure gradient along streamwise and spanwise, thus affecting the boundary layer evolution on the blade surface and endwall, making the domination of low momentum fluid varies. Considering that the location of high entropy low momentum fluid can be revealed by the total pressure loss contours, Figure 8 to 10 provides the total pressure loss in the measurement plane under different incoming flow incidence angles, in comparison of datum and end slotted blade. All the diagrams indicate that the highest total pressure loss occurs in the region of the corner vortices.

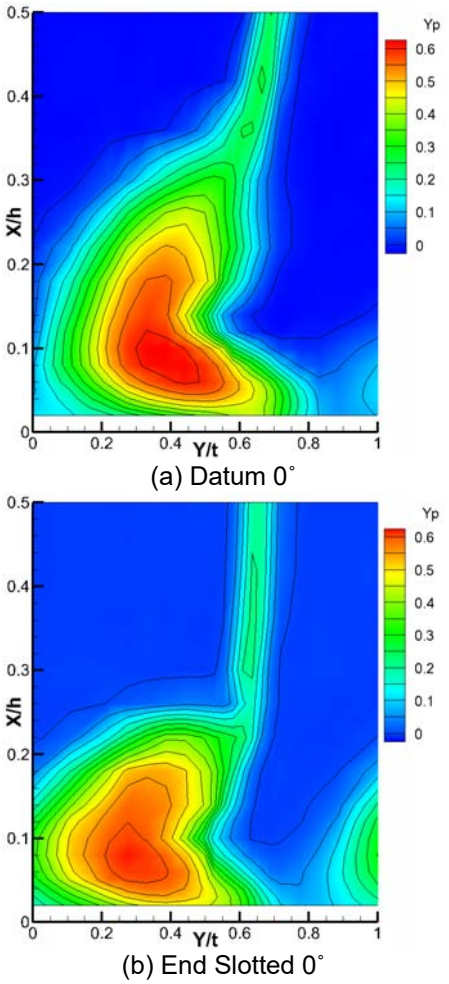

Figure 8. Measurement Plane Total Pressure Loss Contours under the incidence 0˚

For the datum blade under the incidence 0˚, a blockage as bulk as over two thirds in the spanwise of the passage is revealed, shown in Figure 8 (a), while the wake remains narrow. Figure 8 (b) illustrates that the blockage is reduced to lower than 25% span height through the employment of end slots, and the high loss core moves against the blade suction side.

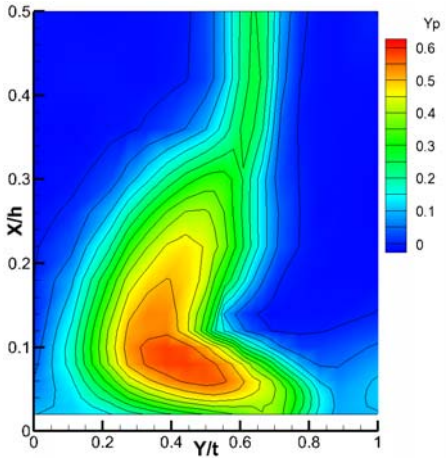

(a) Datum 2˚

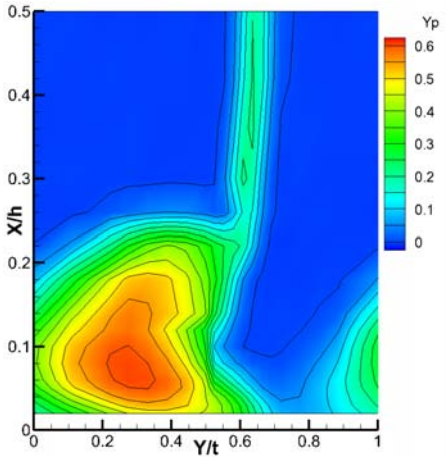

(b) End Slotted 2˚

Figure 9. Measurement Plane Total Pressure Loss Contours under the incidence 2˚

As the incidence increasing, the wake center of the datum blade moves opposed to the blade suction side with the wake width expanded. The separation region has a tendency of growing upward from the incidence 2˚, expressing as the widening in the wake visualized by Figure 9 (a). For the end slotted blade, the separation scale nearly remains, but the loss in the high loss core is reduced.

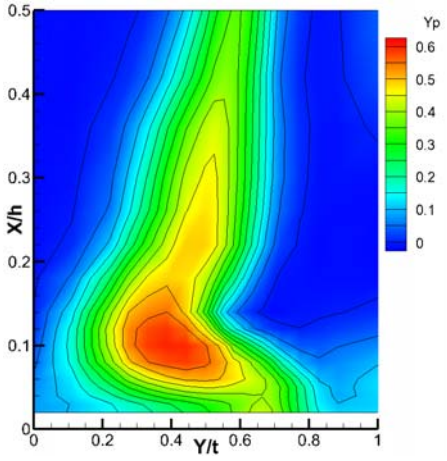

(a) Datum 4˚

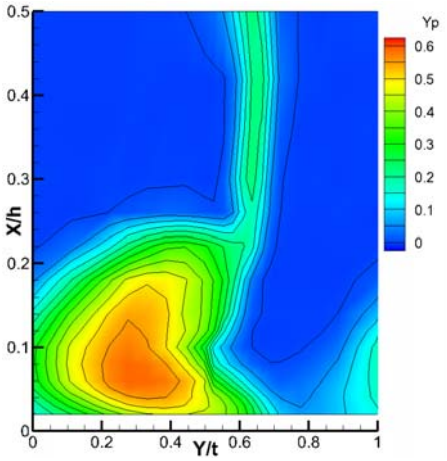

(b) End Slotted 4˚

Figure 10. Measurement Plane Total Pressure Loss Contours under the incidence 4˚

As it shown in Figure 10 (a) that the whole passage stall occurs for the datum blade under the incidence angle of 4˚ with the total pressure loss enlarges aggressively. The adoption of the blade end slots can put forward the appearance of whole passage stall.

As contoured from Figure 8 to 10, the corner separation is effectually restrained by blade end slots. The adaptive outflow from the blade end slots increase the flow momentum in the corner region, and pushes the accumulated low momentum flow downstream, restrains its upward migration along the blade suction surface, contributing to the reduction of blockage at last. Besides, it is noted from the comparison under the incidence of 2˚ and 4˚ (Figure 9 and Figure 10) that the blade end slots is conducive to enhancing the two-dimensionality in the mid-span region of the blade.

In order to gain more understanding of the insight mechanism by which the blade end slots restrain corner separation, the main secondary vortex structures featuring the corner separation are analyzed based on the measurement plane loss distributions. Through the corner separation mechanism analysis from Liu at al [20] based on the delayed detached eddy simulation (DDES), it is thought that the passage vortex is the main secondary vortex and obviously enhances the corner separation. As Kang established in Figure 12 [21] that the passage vortex (PV), concentrated shedding vortex (SCV) and corner vortex (CV) are the main vortex structures that featuring the corner separation.

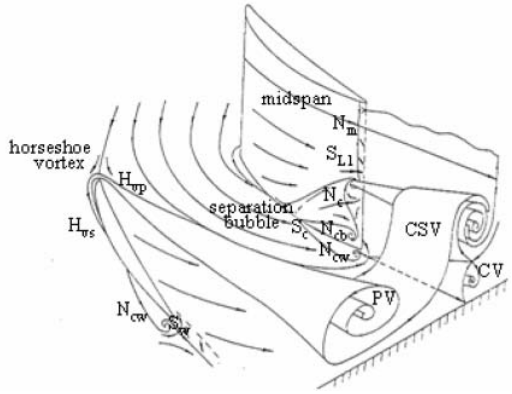

Figure 11. The Main Vortex Structures in the blade-endwall conjunction [21]

The intensity of LE horseshoe vortex and the pressure gradient of the endwall cross flow contribute to the generation and evolution of passage vortex in the blade passage. With the incidence angle increasing, the vortex core of the passage vortex lifts off from the endwall. Reflecting on the development of the high loss core regions, shown from Figure 8 to Figure 10. The adaptive jet flow from the blade end slots energizes momentum to the local low momentum fluid and pushes the high loss core away from the blade suction surface and prevents it from lifting upwards. So the separation structures of the end slotted blade is pushed downstream and restrained in the blade root region, expressing as the expansion in the proportion of the main flow region. Since the position of the high loss core is so adjacent to the endwall in such incoming flow conditions that the designed end slot height is relatively higher, indicating that the reorganization of the blade-endwall corner flow is not the best. Thus, it is of great meaning to further optimize the end slots scheme.

Another high loss region above to the largest loss region results from the SCV in accordance to Figure11, is caused by the involving of the suction side flow over the accumulated low momentum corner with the attached flow from the pressure surface. The high momentum end slot jets energize the local low momentum flow and effectively restrain its accumulation at the blade-endwall corner, so that the partial deflection is impaired, reflecting in the suppression of the high loss region both in the strength and its upward migration at last. In a word, considerable decreases in the corner separation extent and relatively narrower wake rewards as a consequence.

4. Conclusions

The blade end slots effect on a highly loaded high-turning compressor cascade under a typical subsonic Mach number conditions is investigated experimentally in the present paper. Through the detailed comparison of the typical results, conclusions can be drawn below:

- The employment of the blade end slot makes significant contribution to the reduction of corner separation. Prominent potential is shown in broadening the effective operating range positively forward, equipped the blade with better aerodynamic performance.
- The blade end slot is conducive to enhance the two-dimesionality in the mid-span region of the blade, resulting in the enlargement of the main flow region in the middle with the whole capacity aggressively improved.
- Reduced deviation angle and uniformed deviation angle distribution along the spanwise downstream the blade is achieved by the blade end slots.
- The adaptive jet flow from the blade end slots adds momentum to the local low momentum fluid and pushes the high loss core away from the blade suction surface , prevents it from lifting upwards, expressing as the expansion in the proportion of the main flow region.
- The high momentum end slot jets energize the local low momentum flow, effectively restrains its accumulation at the blade-endwall corner and its spanwise migration along the suction surface, reflecting in the suppression of high loss region and its upward migration at last.

Considerable benefits in the suppression of corner separation by blade end slots are validated experimentally with detailed analysis of its control mechanism. Further investigations could be conducted on the end slots scheme optimization.

ACKNOWLEDGMENTS

This work is supported by the National Natural Science Foundation of China (No. 51676007, No. 51420105008, No. 51376001), the National Basic Research Program of China (No. 2014CB046405). Yangwei Liu is supported by the China Scholarship Council (CSC) for a one-year visit to the University of Cambridge.

REFERENCES

[1] V. M. Lei, Z. S. Spakovszky and E. M. Greitzer. A criterion for axial compressor hub-corner stall. *Journal of Turbomachinery*, 130:031006, 2008.

[2] J. D. Denton. Loss mechanisms in turbomachines. *Journal of Turbomachinery*, 115:621-656, 1993.

[3] J. V. Taylor, R. J. Miller. Competing three dimensional mechanisms in compressor flows. *Journal of Turbomachinery ,* 139: 021009, 2017.

[4] S. A. Gbadebo, N. A. Cumpsty and T. P. Hynes. Control of three-dimensional separation in axial compressor by Tailored boundary layer suction. *Journal of Turbomachinery*, 130:011004, 2008.

[5] Y. Liu, J. Sun, L. Lu. Corner Separation Control by Boundary Layer Suction Applied to a Highly Loaded Axial Compressor Cascade. *ENERGIES,* (7): 7994-8007, 2014.

[6] Y. H. Li, Y. Wu and M. Zhou. Control of the corner separation in a compressor cascade by steady and unsteady plasma aerodynamic actuation. *Experiments in Fluid*, 48:1015-1023, 2010.

[7] E. Akcayoz, H. D. Vo, A. Mahallati. Controlling corner stall separation with plasma actuators in a compressor cascade. *Journal of Turbomachinery,* 138: 081008, 2016.

[8] M. Staats, W. Nitsche. Active control of the corner separation on a highly loaded compressor cascade with peridoc nonsteady boundary conditions by means of fluidic actuators. *Journal of Turbomachinery,* 138: 031004, 2016.

[9] M. G. De Giorgi, C. G. D. Luca and A. Ficarella. Comparison between synthetic jets and continuous jets for active flow control: application on a NACA 0015 and a compressor stator cascade. *Aerospace Science and Technology*, 43:256-280, 2015.

[10] S. Evans, H. Hodson and T. Hynes. Flow control in a compressor cascade at high incidence. *Journal of Propulsion and Power*, 26(4):828-836, 2010.

[11] A. J. Wennerstrom. Some experiments with a supersonic axial compressor stage. *Journal of Turbomachinery*, 109(3):388-397, 1987.

[12] M. Ramzi, G. Bois, G. Abderrahmane. Numerical study of passive control with slotted blading in highly loaded compressor cascade at low Mach number. *International Journal of Fluid Machinery and Systems*, 4(1): 97-103, 2011.

[13] W. Hage, R. Mayer and C. Paschereit. Control of secondary flow in a highly loaded compressor stage by means of a groove structure on the sidewalls. *AIAA Paper*, 2007-4278, 2007.

[14] A. Hergt, R. Mayer and K. Engel. Effects of vortex generator application on the performance of a compressor cascade. *Journal of Turbomachinery*, 135(2):021026, 2012.

[15] D. Nerger, H. Saathoff, R. Radespiel, et al. Experimental investigation of endwall and suction side blowing in a highly loaded compressor stator cascade. *Journal of Turbomachinery*, 134: 021010, 2012.

[16] Y. Liu, J. Sun and Y. Tang. Effect of slot at blade root on compressor cascade performance under different aerodynamic parameters. *Applied Sciences*, 6(12):421, 2016. [15] Y. Liu, J. Sun and Y. Tang. Effect of slot at blade root on compressor cascade performance under different aerodynamic parameters. *Applied Sciences*, 6(12):421, 2016.

[17] A. D. Scillitoe, P. G. Tucker, P. Adami. Numerical investigation of three-dimensional separation in an axial flow compressor: the influence of freestream turbulence intensity and endwall boundary layer state. *Journal of Turbomachinery*, 139: 021011, 2017.

[18] G. S. Jones, A. E. Viken, L. N. Washburn, L. N. Jenkins, C. M. Cagle. An active flow circulation controlled flap concept for general aviation aircraft applications. *AIAA Paper*, 2002-3157, 2002.

[19] M. N. Goodhand, R. J. Miller. The impact of real geometries on three-dimensional separations in compressors. *Journal of turbomachinery,* 134(2): 021007, 2012.

[20] Y. Liu, H. Yan, L. Lu, Q. Li. Investigation of Vortical Structures and Turbulence Characteristics in Corner Separation in a Linear Compressor Cascade Using DDES. *JOURNAL OF FLUIDS ENGINEERING-TRANSACTIONS OF THE ASME,* 139(2), 2017.

[21] S. Kang. Investigation of the Three Dimensional Flow within a Compressor Cascade with and without Tip Clearance. *Ph.D. Thesis,* Dept. of Fluid Mechanics, Vrije Universiteit Brussel. I-1-V-44, 1993.